Cellular and Molecular Life Sciences (2021) 78:7831–7849
https://doi.org/10.1007/s00018-021-03972-x

ORIGINAL ARTICLE

α-Klotho released from HK-2 cells inhibits osteogenic differentiation of renal interstitial fibroblasts by inactivating the Wnt–β-catenin pathway

Zewu Zhu[1] · Shuhao Ruan[1] · Yingcheng Jiang[1] · Fang Huang[1] · Weiping Xia[1] · Jinbo Chen[1] · Yu Cui[1] · Cheng He[1] · Feng Zeng[1] · Yang Li[1] · Zhiyong Chen[1] · Hequn Chen[1]

Received: 1 June 2021 / Revised: 18 August 2021 / Accepted: 6 September 2021 / Published online: 1 November 2021

Abstract

Randall's plaques (RP) are well established as precursor lesions of idiopathic calcium oxalate (CaOx) stones, and the process of biomineralization driven by osteogenic-like cells has been highlighted in RP formation, but the mechanism is poorly understood. Given the inhibitory role of α-Klotho (KL), an aging suppressor protein with high expression in kidneys, in ectopic calcification and the close association between *KL* gene polymorphisms and urolithiasis susceptibility, we determined the potential role of KL in RP formation. This study found that both soluble KL (s-KL) and transmembrane KL (m-KL) were downregulated, and that s-KL but not m-KL was inversely correlated with upregulation of osteogenic markers in RP tissues. Additionally, s-KL expression was markedly suppressed in human renal interstitial fibroblasts (hRIFs) and slightly suppressed in HK-2 cells after osteogenic induction, intriguingly, which was echoed to the greater osteogenic capability of hRIFs than HK-2 cells. Further investigations showed the inhibitory effect of s-KL on hRIF osteogenic differentiation in vitro and in vivo. Moreover, coculture with recombinant human KL (r-KL) or HK-2 cells suppressed osteogenic differentiation of hRIFs, and this effect was abolished by coculture with *KL*-silenced HK-2 cells or the β-catenin agonist SKL2001. Mechanistically, s-KL inactivated the Wnt–β-catenin pathway by directly binding to Wnt2 and upregulating SFRP1. Further investigations identified activation of the Wnt–β-catenin pathway and downregulation of SFRP1 and DKK1 in RP tissues. In summary, this study identified s-KL deficiency as a pathological feature of RP and revealed that s-KL released from HK-2 cells inhibited osteogenic differentiation of hRIFs by inactivating the Wnt–β-catenin pathway, not only providing in-depth insight into the role of s-KL in renal interstitial biomineralization but also shedding new light on the interaction of renal tubular epithelial cells with interstitial cells to clarify RP formation.

Keywords α-Klotho · β-catenin · Osteogenic differentiation · Renal interstitial fibroblasts · HK-2 · Randall's plaques

Abbreviations

ARS	Alizarin Red staining
ALP	Alkaline phosphatase
CaOx	Calcium oxalate
CaP	Calcium phosphate
CaOx-SF	CaOx stone formers
HC	Healthy controls
hRIFs	Human renal interstitial fibroblasts
KL	*KLOTHO*
NRP	Normal renal papillae
RP	Randall's plaques
r-KL	Recombinant human KL
SFRPs	Secreted Frizzled-related proteins
s-KL	Soluble α-Klotho
m-KL	Transmembrane α-Klotho
UKCR	Urinary s-KL-to-creatinine ratio

✉ Zhiyong Chen
jeffastone@126.com

✉ Hequn Chen
chenhequnxy@126.com

[1] Department of Urology, Xiangya Hospital, Central South University, Changsha 410008, Hunan, China

Introduction

Nephrolithiasis affects nearly 10% of the population and has an increasing prevalence worldwide [1–3], and the most common composition of nephroliths is calcium oxalate (CaOx) [4]. With the development and widespread use of

endoscopy, an increasing number of studies have confirmed the close association between CaOx stones and Randall's plaques (RP) [5, 6], identified in 1937 by Dr. Alexander Randall [7]. Currently, it is believed that the formation of RP and their development into a nidus for CaOx stones occurs in at least three phases: initial deposition of calcium phosphate (CaP) crystals in the papillary interstitium, aggregation and growth, and breaching of the covering epithelium [8]. Moreover, extensive evidence indicates that RP formation shares similarities with biomineralization driven by osteogenic-like cells [9–11]; however, the precise underlying mechanism is not fully elucidated [12].

KLOTHO (*KL*) has been established as an aging suppressor gene [13, 14] that encodes the α-Klotho (KL) protein, which is expressed at a high level in the kidneys, brain choroid plexus and parathyroid glands [13, 15, 16]. Recent evidence has indicated that the human KL protein has only 2 forms with potentially different functions, namely, full-length transmembrane KL (m-KL; ~ 135 kD) and soluble KL (s-KL; 60–70 kD or ~ 130 kD) resulting from proteolytic cleavage of m-KL [17–20], because a paradigm-shifting study revealed that the alternatively spliced mRNA previously proposed to encode the truncated secreted isoform of KL was not translated but was instead a target for nonsense-mediated mRNA decay in humans [19]. s-KL can enter the blood and urine and was identified as the circulating form of KL that acts as a hormone to regulate other cells and tissues [21]. Mice with a loss-of-function mutation in *Kl* ($Kl^{-/-}$) showed a wide spectrum of organ disorders resembling human aging; conversely, *Kl* overexpression attenuated these disorders and extended the lifespan [22, 23]. One of these disorders was severe soft tissue calcification including aortic valve calcification and nephrocalcinosis in mice with *Kl* deletion throughout the nephron ($Six2\text{-}Kl^{-/-}$) [15]. In recent decades, numerous studies have determined the potential role of KL in calcification. KL was found to suppress the osteogenic process in human aortic valve interstitial cells (AVICs) induced by high phosphate [24] and to inhibit osteogenic differentiation of human bone marrow mesenchymal stem cells (BMSCs) in vitro [25], indicating that it plays an inhibitory role in osteogenic differentiation. Interestingly, *KL* gene polymorphisms were found to be associated with susceptibility to both cardiovascular disease and urolithiasis in the general population, without racial dependency [26]. However, regrettably, few studies have investigated whether KL mediates renal interstitial biomineralization to participate in RP formation.

KL is highly expressed in renal tubular epithelial cells [27], and RP have been identified to originate from CaP crystal deposition under the tubular basement membrane of the loop of Henle [28]. Our previous study indicated that osteogenic differentiation of human renal interstitial fibroblasts (hRIFs) might mediate RP formation [29]. Theoretically, integrated investigation of cellular interactions rather than the study of a single population of cells will provide new insights into the pathogenic mechanisms underlying of RP formation at a kidney-wide level. Therefore, this study aimed to determine (1) the expression of s-KL and m-KL in RP; (2) the potential role of s-KL in hRIFs during osteogenic induction; (3) whether recombinant human KL (r-KL) impairs osteogenic differentiation of hRIFs; and (4) whether s-KL released from human renal proximal tubular cells (HK-2 cells) inhibits osteogenic differentiation of hRIFs.

Materials and methods

Clinical samples

After obtaining approval from the Xiangya Hospital Ethics Committee (Approval Number: 202103089) and written informed consent from all participants, we obtained RP tissues from idiopathic CaOx stone formers (CaOx-SF) during percutaneous nephrolithotomy and normal renal papillae (NRP) from patients undergoing nephrectomy due to upper urinary tract cancer, as reported in our previous study [29]. Additionally, we determined the s-KL concentration in morning urine samples collected from adult CaOx-SF and healthy controls (HC) in the health examination center of our hospital. The inclusion criteria for CaOx-SF were as follows: (1) no renal dysfunction; (2) absent or mild hydronephrosis; and (3) no renal atrophy as determined by computed tomography. HC were defined as those who met the following criteria, at a minimum: (1) normal renal function without congenital kidney malformation or nephritis; (2) no history of urolithiasis, hydronephrosis or upper urinary tract surgery; (3) the absence of proteinuria or hematuria; and (4) the absence of hypertension or diabetes mellitus.

Cell isolation, culture and osteogenic differentiation

HRIFs were isolated and identified in accordance with methods reported in our previous study [29], and hRIFs between passages 3 and 6 were selected for further experiments. HK-2 cells were purchased from the Advanced Research Center of Central South University (Changsha, China). Cells were cultured in DMEM (BI, Israel) supplemented with 10% fetal bovine serum (BI, Israel), 100 U/mL penicillin and 100 μg/mL streptomycin (BI, Israel) at 37 °C in the presence of 5% CO_2. Osteogenic differentiation was induced with widely used osteogenic medium as reported in previous studies [29, 30].

For coculture with r-KL (Glu34(E)-Ser981(S); R&D Systems; USA), r-KL was added to the medium at a concentration of 200 ng/ml for the time indicated in the experiment descriptions. For coculture with HK-2 cells, HK-2 cells (8

$\times 10^4$ cells/cm^2) were seeded in the upper chamber of the coculture plate (0.4 μm; Corning, USA), and hRIFs (4×10^4/cm^2) were seeded in the lower chamber.

ELISA of s-KL in urine samples and cell supernatants

Urine samples and cell supernatants were centrifuged for 5 min at 3000 rpm (4 °C) to remove particulate matter, and the concentration of s-KL was determined by ELISA using Human s-KL Assay Kits (IBL, Japan), which can detect s-KL containing KL1 + KL2 or KL1, according to the manufacturer's instructions [31]. The intra-assay coefficient of variation (CV) and inter-assay CV ranged from 2.7 to 3.5% and from 2.9 to 11.4%, respectively. The standard curve ranging from 46.825 to 3000 pg/mL was well established (R^2: 0.983–0.994). The concentration of urinary s-KL was normalized to that of urinary creatinine (Cr) and was expressed as the urinary s-KL-to-creatinine ratio (UKCR). Cell culture medium was used as a negative control for analysis of cell supernatants s-Kl. The concentration of supernatant s-KL was calculated by subtracting the value of the negative control, and the total volume of medium in each well was also taken into consideration to obtain the normalized concentration.

Cell transfection

To overexpress or silence *KL*, recombinant lentiviruses carrying the sequence of *KL* (Len-*KL*) or shRNA targeting *KL* (Len-sh-*KL*), purchased from GenePharma (Shanghai, China), was used to transfect hRIFs and HK-2 cells. The transfected hRIFs and HK-2 cells were selected with 2 μg/ml puromycin for 5 days and 3 μg/ml puromycin for 7 days, respectively. Additionally, a plasmid expressing *Wnt2* (pHA-*Wnt2*; GV366; GenePharma, China) was constructed and used to overexpress *Wnt2*, and siRNAs (RiboBio, China) were used to silence *SFRP1* (si-*SFRP1*) or *SFRP4* (si-*SFRP4*) via transfection with Lipofectamine 2000 (Invitrogen, USA) according to the manufacturer's protocols. The primer sequences designed for overexpression of *KL* and *Wnt2* are listed in Supplementary Table 1, and the sequences of the shRNA for *KL* and the siRNAs for *SFRP1* or *SFRP4* are listed in Supplementary Table 2.

Immunohistochemistry (IHC)

IHC on NRP and RP tissues was performed with standard techniques as reported in our previous study [29]. The details of the specific primary antibodies are as follows: anti-s-KL (1:500; ab181373, Abcam, UK); anti-m-KL (1:400; 28,100–1-AP, Proteintech, China); anti-osteocalcin (OCN; 1:400; ab93876; Abcam, UK); anti-MSX2 (1:200; ab69058, Abcam, UK); anti-Runx2 (1:300; #12,556, CST, USA); anti-β-Catenin (1:500; 51,067–2-AP, Proteintech, China); anti-DKK1 (1:300; ab109416, Abcam, UK); anti-SFRP1 (1:300; ab126613, Abcam, UK); and anti-SFRP4 (1:500; ab154167, Abcam, UK). As described in a previous study [32], images of DAB staining (400×) were quantitatively analyzed with the IHC Toolbox plugin in ImageJ [33]. The color threshold for the average gray value was set to a value between 0 and 254. A value of 0 was used for a black, dark-stained area, and a value of 254 was used for a white, unstained area, leading to an inverse correlation between the DAB staining intensity and the average gray value.

Reverse transcription and quantitative real-time polymerase chain reaction (qRT-PCR)

Total RNA was isolated using TRIzol reagent (Takara, Japan). Reverse transcription was performed using a PrimeScript RT Reagent Kit (Takara, Japan); qRT-PCR was performed using SYBR Green PCR Reagent (Takara, Japan) in a real-time PCR instrument (Applied Biosystems, USA) according to the manufacturer's instructions. Relative gene expression levels were calculated using the $2^{-\Delta\Delta Ct}$ method with normalization to the levels of GAPDH in control samples. The primers are listed in Supplementary Table 3. Additionally, the PCR products amplified by each pair of primers were verified by 2% agarose gel electrophoresis (Supplementary Fig. 1).

Western blotting (WB)

Total protein was extracted using RIPA lysis buffer (Beyotime, China) containing 1% PMSF and 1% ProtLytic Phosphatase Inhibitor Cocktail (NCM Biotech, China). After measuring the protein concentration with a BCA Kit (Beyotime, China), equal amounts of total protein were loaded onto 12% SDS-PAGE gels (GenScript, China) and separated by electrophoresis prior to transfer to 0.45 μm PVDF membranes. After blocking, membranes containing the target proteins were incubated with primary antibodies at 4 °C overnight prior to washing and incubation with the corresponding horseradish peroxidase-conjugated secondary antibody. Blots were visualized using chemiluminescence reagents (NCM Biotech; China) in a ChemiDoc XRS imaging system (Bio-Rad, USA). The gray value of each band was calculated with ImageJ software, and the relative expression level was calculated by normalization to GAPDH. The details of the antibodies used for WB are listed in Supplementary Table 4.

Cell immunofluorescence

HRIFs were seeded on coverslips at a confluence of approximately 25% and treated with osteogenic medium for 3 days.

The cell layer was washed with cold PBS 3 times prior to fixation with 4% paraformaldehyde (PFA) for 20 min. After blocking with 10% normal goat serum (Solarbio, China) for 1 h at room temperature, slides were incubated with primary antibodies against s-KL (1:200; ab181373, Abcam, UK) or Wnt2 (1:400; 66,656–1-Ig, Proteintech, China) at 4 °C overnight. Slides were washed with cold PBS and were then incubated with secondary antibodies conjugated to Alexa Fluor 488 (1:800; ab150077, Abcam, UK) or 647 (1:500; ab150115, Abcam, UK) for 1 h at room temperature prior to the addition of DAPI (Service, China) for 5 min. Images were acquired with a confocal microscope (Leica TCS SP8 X, Germany).

Coimmunoprecipitation (Co-IP)

Co-IP was performed to determine the interaction of s-KL with Wnt ligands in hRIFs, as previously reported [27]. The anti-s-KL antibody (ab181373, Abcam, UK) was conjugated to protein A/G Plus Magnetic Agarose Beads (Millipore, USA) at room temperature for 1 h prior to immunoprecipitation at 4 °C overnight with lysates of hRIFs transfected with Len-*KL*. After washing with lysis buffer 3 times, the precipitated complexes were immunoblotted with specific antibodies, as described in WB.

Alizarin Red staining (ARS) and alkaline phosphatase (ALP) activity measurement

The cell layer was washed with PBS twice prior to fixation with 4% PFA for 30 min. After washing the layer with ddH_2O twice, 1% Alizarin Red (pH = 4.2, Solarbio, China) was used to stain the layer for 10 min, after which calcified nodules were visualized as orange–red spots. After washing the layer with ddH_2O 3 times, images were acquired with an inverted microscope (Leica, Germany).

ALP activity measurement was performed using an ALP colorimetric assay kit (Beyotime, China) in accordance with the manufacturer's instructions. Briefly, lysis buffer was added to cell layers after washing with cold PBS, and the ALP activity in the lysates was determined by measuring the absorbance at 405 nm indicating the release of p-nitrophenol.

TOPFlash luciferase reporter assay

The TOPFlash plasmid (Millipore, USA) carries two sets of three copies of T cell factor (TCF) binding sites upstream of the firefly luciferase gene. As described in previous studies [27, 34], the TOPFlash luciferase reporter assay is often used to evaluate effects on β-catenin-dependent activation of the Wnt/β-catenin pathway. In brief, hRIFs were cotransfected with the TOPFlash plasmid and Renilla luciferase plasmid as an internal control with Lipofectamine 2000 (Invitrogen, USA) according to the manufacturer's protocols. Transfected hRIFs were cocultured with r-KL or HK-2 cells under osteogenic conditions. A dual-luciferase reporter assay system kit (Promega, USA) was used to measure luciferase activity. The fold change in the relative luciferase (firefly luciferase/Renilla luciferase) activity was calculated to assess activation of the Wnt/β-catenin pathway.

Subcutaneous ectopic transplantation of hRIFs in vivo

After obtaining approval from the Institutional Experimental Animal Committee of Central South University (Proof Number: 2021sydw0033), 9 female nude mice (8 weeks old) obtained from the Animal Experimental Center of Central South University were used in this study, and all efforts were made to reduce the suffering and number of mice. HRIFs with or without lentiviral transduction were induced with OM for 14 days before transplantation. Next, 1×10^7 cells were seeded on 8.5 mm × 5 mm × 1.5 mm hydroxyapatite (HA) scaffolds, which were purchased from Hengtian Biotechnology Co., Ltd. (Zhuzhou, China). Six groups of grafts were implanted subcutaneously on the dorsal surface of mice under general anesthesia: the blank group (HA without cells), the normal control (NC) group (HA with hRIFs), the Len-sh-ctrl group (HA with hRIFs transfected with Len-sh-ctrl), the Len-sh-*KL* group (HA with hRIFs transfected with Len-sh-*KL*), the Len-ctrl group (HA with hRIFs transfected with Len-ctrl) and the Len-*KL* group (HA with hRIFs transfected with Len-*KL*). All samples were collected 8 weeks after transplantation and were then fixed with 4% paraformaldehyde for 72 h. After dehydration with gradient alcohol and transparent with xylene, the samples were embedded in 15.7% methyl methacrylate (MMA) for 72 h, and 10 μm thick tissue sections were prepared using a hard tissue slicer (HistoCore AUTOCUT, Germany). After dewaxing with ethylene glycol ethyl ether acetate (EGEEA) and rehydration, hematoxylin and eosin (HE) staining and Masson's trichrome staining were performed via conventional protocols for histological examination.

Statistical analysis

Categorical data were analyzed by the chi-square or Fisher's exact test; continuous data expressed as mean ± standard deviation values were analyzed by Student's *t* test or one-way analysis of variance (ANOVA), as appropriate. Correlations between parameters were analyzed by Pearson rank correlation. GraphPad Prism (version 8.0, La Jolla, CA, USA) was used to perform all statistical analyses, and a two-sided P value < 0.05 was considered to indicate statistical

significance. In all comparisons, *, **, and *** were defined as $p < 0.05$, 0.01, and 0.001, respectively.

Results

s-KL and m-KL were downregulated in RP

To investigate whether KL is involved in RP formation, we analyzed the expression of KL in RP and NRP samples as well as in urine from CaOx-SF and HC. The clinical features of the included patients and controls are shown in Supplementary Table 5 and Supplementary Table 6. Both *KL* mRNA (RP = 30, NRP = 30) and protein expression (s-KL, m-KL, RP = 18, NRP = 18) were significantly decreased in RP (Fig. 1A–1D, Fig. 7I–7K, M, Supplementary Fig. 2A), and we noted a trend of UKCR downregulation in CaOx-SF ($n = 30$) compared with HC ($n = 30$), but the difference was not significant (Fig. 1E). Additionally, osteogenic protein markers (Runx2, MSX2, and OCN) were upregulated in RP (Fig. 1B–1D, Supplementary Fig. 2A), consistent with our previous studies [29]. Interestingly, linear regression analysis showed that s-KL protein expression was positively correlated with that of m-KL (Supplementary

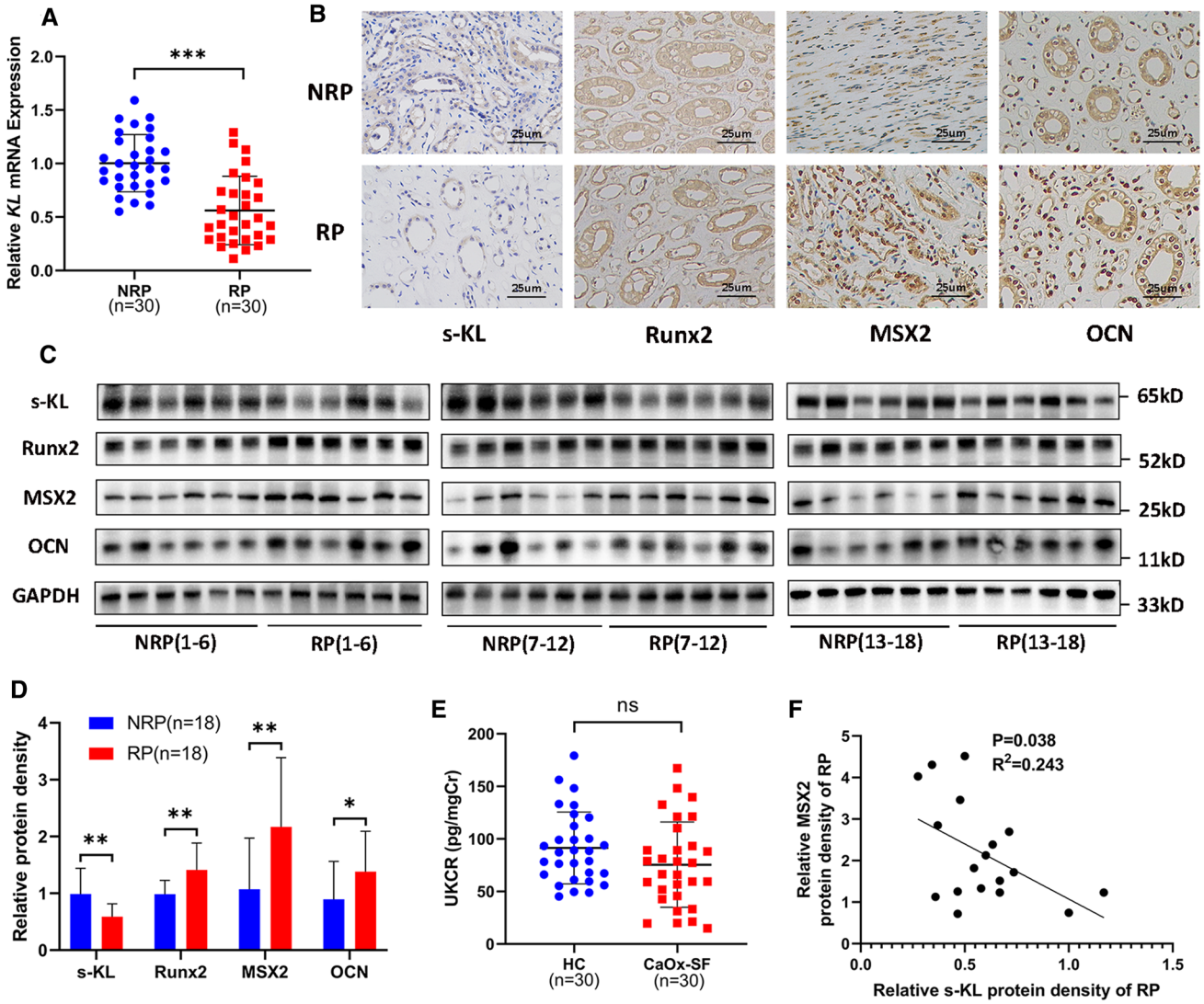

Fig. 1 Soluble α-Klotho (s-KL) and osteogenic markers (OCN, MSX2, and Runx2) in Randall's plaques (RP) and normal renal papillae (NRP). **A** *KL* mRNA expression measured by qRT-PCR in RP ($n = 30$) and NRP ($n = 30$) tissues. **B** Immunohistochemistry (IHC) for s-KL and osteogenic markers in RP ($n = 6$) and NRP ($n = 6$) tissues. **C–D** Representative western blots and quantification of s-KL and osteogenic marker levels in RP ($n = 18$) and NRP ($n = 18$) tissues. **E** Urinary s-KL was determined by ELISA in healthy controls (HC; $n = 30$) and CaOx stone formers (CaOx-SF; $n = 30$), and the concentration was expressed as the urinary s-KL-to-creatinine ratio (UKCR). **F** Correlation analysis between the relative protein expression levels of s-KL and MSX2 in RP tissues; $n = 18$

Fig. 2B) and negatively correlated with that of MSX2 among the osteogenic markers (Fig. 1F, Supplementary Fig. 2C–D), but there was no significant correlation between the expression of m-KL and that of any osteogenic protein marker (Supplementary Fig. 2E–G). The above results prompted us to further explore whether s-KL participates in RP formation driven by osteogenic-like cells.

s-KL was downregulated during osteogenic differentiation of hRIFs

Given that interstitial cells and tubular epithelial cells might adopt an osteogenic-like phenotype to participate in RP formation [10, 29], we evaluated the osteogenic capability of hRIFs and HK-2 cells in vitro via induction with osteogenic medium for 14 days. ARS showed that hRIFs (Fig. 2A–B) yielded many more calcium deposits than HK-2 cells (Fig. 2H–I). Consistent with this result, the protein levels of osteogenic markers (Runx2, MSX2, and OCN) in hRIFs were markedly increased in an osteogenic induction time-dependent manner (Fig. 2C, Supplementary Fig. 2H–2 J), while in HK-2 cells, only MSX2 and OCN (Fig. 2J, Supplementary Fig. 2L–2 N) were increased 4 and 7 days after induction. In addition, the relative change in ALP activity was greater in osteogenic-induced hRIFs (Fig. 2D) than in HK-2 cells (Fig. 2K). The above results indicated that hRIFs had a greater osteogenic capability than HK-2 cells. Furthermore, osteogenic induction led to downregulation of s-KL in both hRIFs (Fig. 2C, Supplementary Fig. 2 K) and HK-2 cells (Fig. 2J, Supplementary Fig. 2O), and the s-KL level in hRIFs was significantly decreased in a time-dependent manner. Moreover, linear regression analysis showed that the protein expression levels of MSX2 and Runx2 were negatively correlated with that of s-KL (Fig. 2E–G), indicating that s-KL might participate in regulating osteogenic differentiation of hRIFs.

s-KL attenuated osteogenic differentiation of hRIFs in vitro and in vivo

We further modulated the expression of s-KL in hRIFs using recombinant lentiviruses (Supplementary Fig. 3A–B). Overexpression of s-KL significantly attenuated the osteogenic phenotype (Fig. 3A, B, E–G) and greatly increased the concentration of s-KL in the collected cell supernatants (Fig. 3H), while knockdown of s-KL significantly enhanced the osteogenic phenotype of hRIFs (Fig. 3C–G) and slightly decreased the concentration of s-KL in the cell supernatants under osteogenic conditions (Fig. 3H). To further evaluate the effect of supernatant s-KL on the osteogenic phenotype, hRIFs were cocultured with r-KL under osteogenic conditions. The results showed that r-KL also played an inhibitory role in osteogenic differentiation, and the levels of osteogenic markers were negatively correlated with that of r-KL in an approximately dose-dependent manner (Fig. 3I). Moreover, coculture with r-KL attenuated the osteogenic phenotype of hRIFs that was enhanced by Len-sh-*KL* transfection (Fig. 3J–K).

To further verify the inhibitory effect of KL on osteogenic differentiation, porous HA scaffolds (Fig. 4A–B) containing hRIFs were implanted subcutaneously on the dorsal surface of nude mice (Fig. 4C), as reported in previous studies[35, 36]. Samples were collected for histological examination 8 w after transplantation. HE and Masson staining (Fig. 4D) showed that the samples from the blank group were filled with empty bubble-like structures, while samples from the NC group showed ordered collagen fibers. Moreover, collagen fibers were more abundant in the Len-sh-*KL* group than in the Len-sh-ctrl group, while collagen fibers were less abundant in the Len-*KL* group than in the Len-ctrl group.

s-KL released from HK-2 cells inhibited osteogenic differentiation of hRIFs

Since KL is highly expressed in renal tubular epithelial cells [37] and RP have been reported to originate from CaP deposited under the tubular basement membrane of the loop of Henle [38], we further investigated whether HK-2 cells also plays an inhibitory role in osteogenic differentiation of hRIFs mediated partially via s-KL. First, the relative KL expression levels were compared between hRIFs and HK-2 cells cultured in normal medium. Interestingly, HK-2 cells had significantly higher expression of KL than hRIFs at both the mRNA (Supplementary Fig. 3C) and protein levels (m-KL and s-KL, Supplementary Fig. 3D–E). Next, hRIFs were cocultured with HK-2 cells under osteogenic conditions (Fig. 5A–B). Compared to hRIFs in monoculture, the cocultured cells exhibited a significant increase in the concentration of s-KL in the collected supernatants (Fig. 5C) and decreased expression of osteogenic markers (Fig. 5D–E), and ARS showed significantly decreased calcium deposits in the hRIF layers (Fig. 5A–B). To verify whether s-KL released from HK-2 cells contributes to inhibition of osteogenic differentiation in the coculture system, hRIFs were cocultured with HK-2 cells in which *KL* was overexpressed or knocked down with recombinant lentivirus (Supplementary Fig. 3F–G). Interestingly, coculture with *KL*-overexpressing HK-2 cells largely increased the concentration of s-KL in the cell supernatant (Fig. 5C) and resulted in a further significant decrease in the expression of the osteogenic marker OCN (Fig. 5D–E), while coculture with *KL*-knockdown HK-2 cells significantly decreased the cell supernatant concentration of s-KL (Fig. 5C) and abolished the inhibitory effect (Fig. 5D–E). Therefore, it was

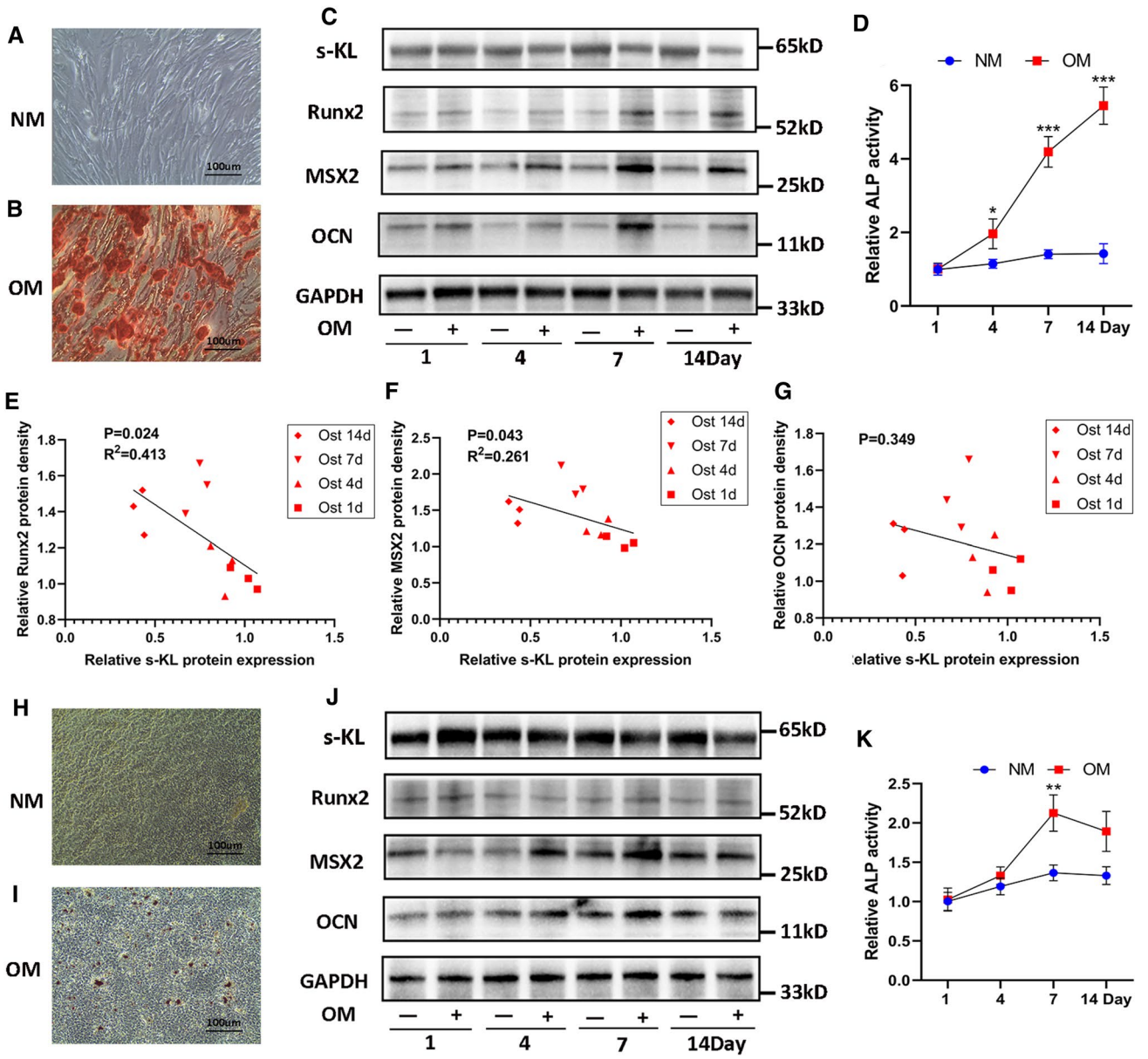

Fig. 2 Soluble α-Klotho (s-KL) was downregulated in osteogenic-induced human renal interstitial fibroblasts (hRIFs) and HK-2 cells. **A** Alizarin Red staining (ARS) for calcium deposits in hRIF layers induced with normal medium (NM) for 14 days; $n=3$. **B** Alizarin Red staining (ARS) for calcium deposits in hRIF layers cultured with osteogenic medium (OM) for 14 days; $n=3$. **C** Representative western blots of s-KL and osteogenic markers (OCN, MSX2, Runx2) in hRIFs 1, 4, 7, and 14 days after culture in either OM or NM; $n=3$. **D** Relative alkaline phosphatase (ALP) activity in hRIF lysates 1, 4, 7, and 14 days after culture in either OM or NM; $n=3$. **E–G** Correlation analysis between the relative protein expression levels of s-KL and osteogenic markers in OM-induced hRIFs. **H** ARS for calcium deposits in HK-2 cell layers cultured with NM for 14 days; $n=3$. **(I)** ARS for calcium deposits in HK-2 cell layers induced with OM for 14 days; $n=3$. **J** Representative western blots of s-KL and osteogenic markers in HK-2 cells 1, 4, 7, and 14 days after culture in either OM or NM; $n=3$. **K** ALP activity in HK-2 cell lysates 1, 4, 7, and 14 days after culture in either OM or NM; $n=3$

reasonable to conclude that HK-2 cells inhibited osteogenic differentiation of hRIFs at least partially through the release of s-KL.

s-KL inactivated the Wnt–β-catenin pathway by binding to Wnt2

Considering the essential role of the Wnt–β-catenin pathway in osteogenic differentiation and the inhibitory effect of s-KL on the Wnt–β-catenin pathway [39, 40],

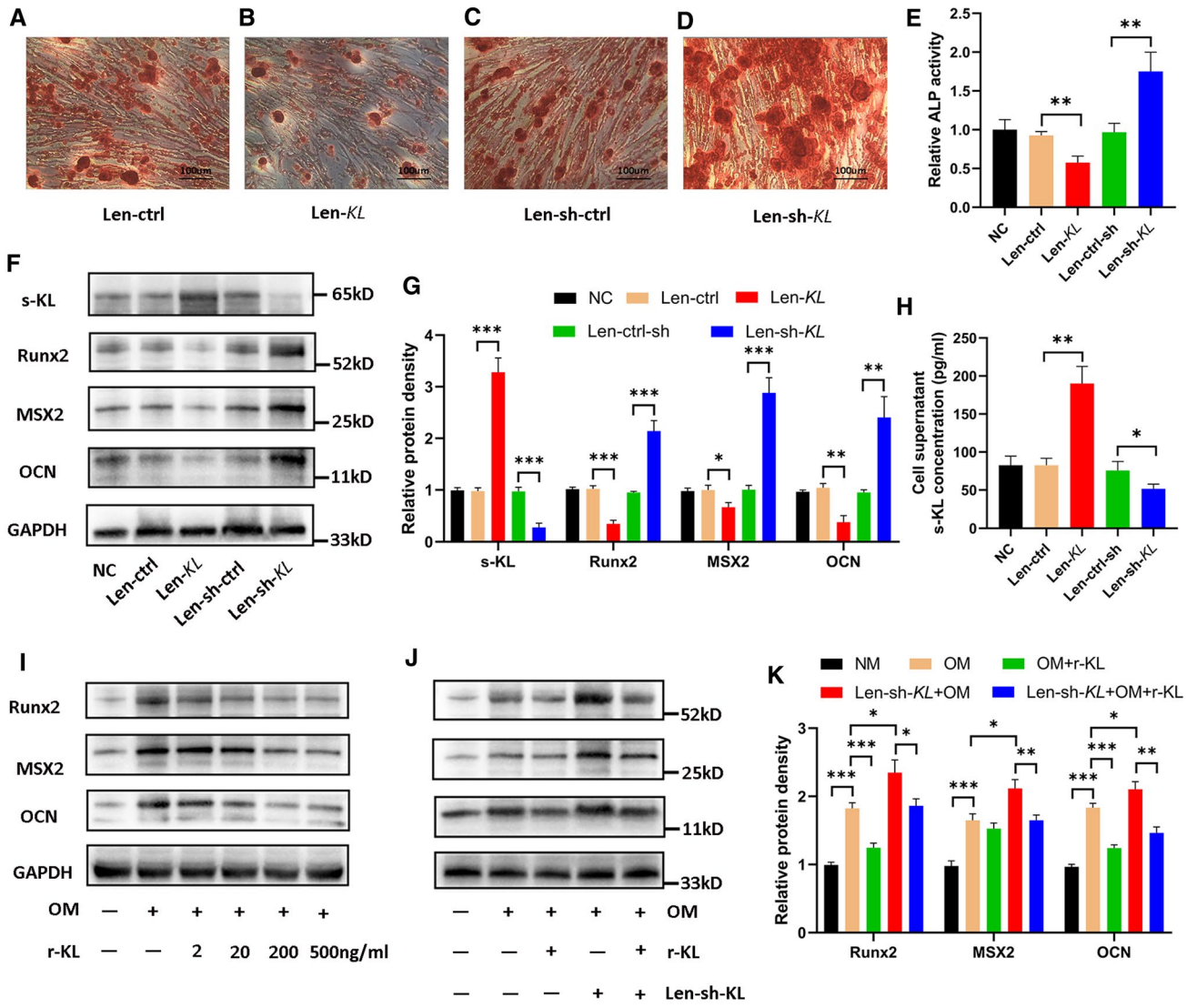

Fig. 3 Soluble α-Klotho (s-KL) inhibited osteogenic differentiation of human renal interstitial fibroblasts (hRIFs). HRIFs were transfected with lentivirus to overexpress or silence s-KL. **A–D** Alizarin Red staining (ARS) of transfected hRIF layers 14 days after osteogenic induction; $n=3$. **E** Relative alkaline phosphatase (ALP) activity in hRIF lysates 7 days after osteogenic induction; $n=3$. **F–G** Representative western blots and quantification of s-KL and osteogenic marker (OCN, MSX2, Runx2) expression in hRIFs 7 days after osteogenic induction; $n=3$. **H** s-KL concentration determined by ELISA in the cell supernatants of hRIFs 7 days after osteogenic induction; $n=6$. **I** Representative western blots of osteogenic markers in hRIFs cocultured with different concentrations of recombinant human KL (r-KL) 7 days after osteogenic induction; $n=3$. **J–K** Representative western blots and quantification of osteogenic marker expression in Len-sh-*KL*-transfected hRIFs cocultured with 200 ng/ml r-KL in osteogenic medium (OM) 7 days after osteogenic induction; $n=3$

we explored whether s-KL attenuates Wnt–β-catenin signaling to inhibit osteogenic differentiation of hRIFs. Our study found that coculture with r-KL or HK-2 cells was able to increase the p-β-catenin/β-catenin ratio (Fig. 5F–G). Since s-KL can directly bind to multiple Wnt ligands to inactivate the Wnt–β-catenin pathway [21], we analyzed the mRNA expression of all identified Wnt ligands in hRIFs under osteogenic conditions by qRT-PCR (Fig. 5H) and found that the mRNA expression levels of *Wnt2*, *Wnt5b* and *Wnt9a* were significantly increased; the protein expression levels as determined by WB were also markedly increased (Fig. 5I–J). Furthermore, Co-IP was used to evaluate the interactions of s-KL with these Wnt ligands. Co-IP assays in whole-cell lysates of Len-*KL*-transfected hRIFs showed that s-KL bound to the Wnt2 protein (Fig. 5K) but not to the Wnt9a (Supplementary Fig. 3H) or Wnt5b (Supplementary Fig. 3I) protein. Subsequently, immunofluorescence staining was performed to determine the subcellular colocalization of s-KL with Wnt2 and discovered that s-KL was partially

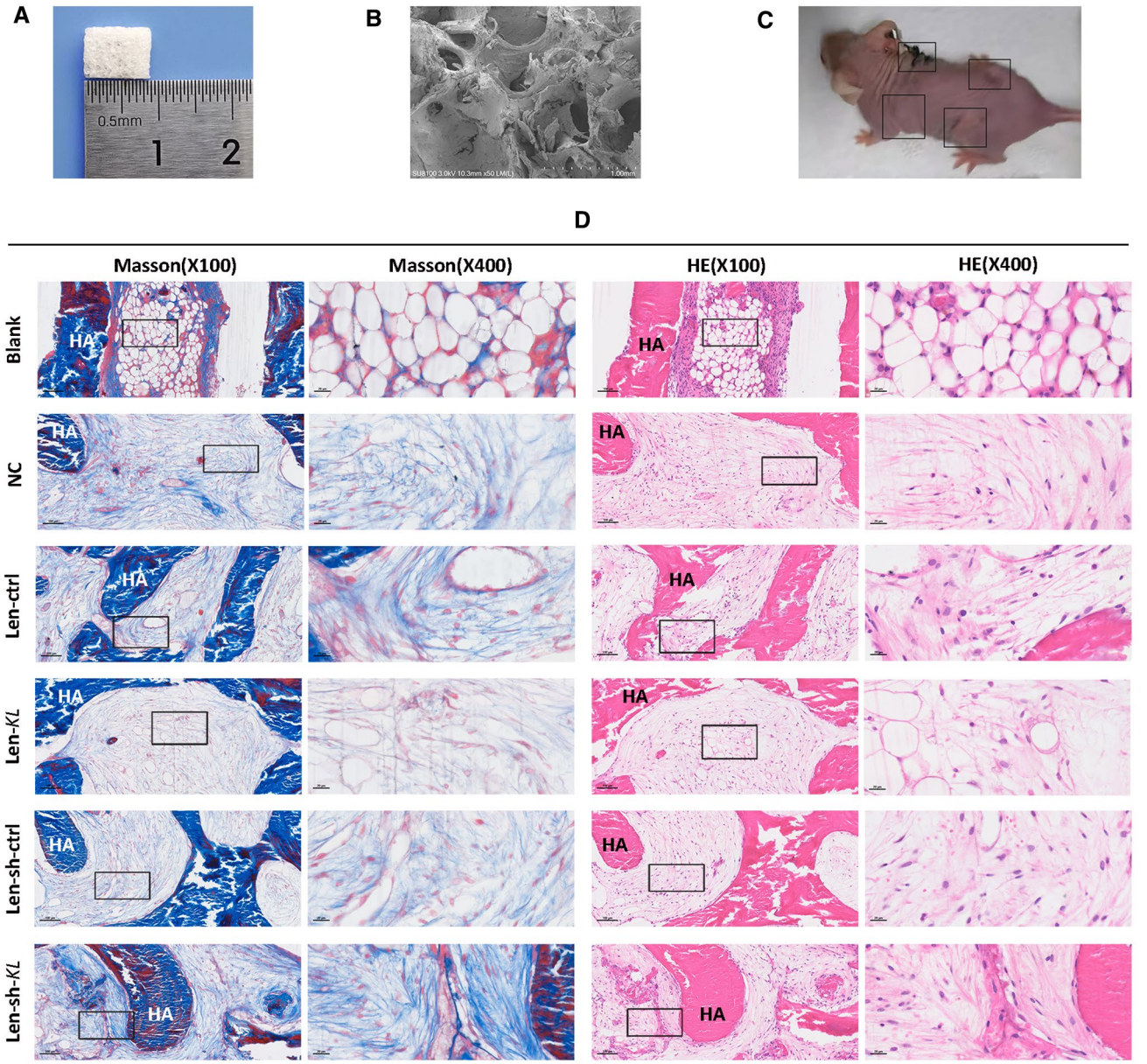

Fig. 4 Hematoxylin and eosin (HE) staining and Masson's trichrome staining for subcutaneously transplanted hydroxyapatite (HA) scaffold materials containing human renal interstitial fibroblasts (hRIFs) in nude mice. **A** A porous HA scaffold material with a size of 8.5 mm × 5 mm × 1.5 mm. **B** The porous structure of HA, as visualized by scanning electron microscopy. **C** Representative picture of a 16-week-old female nude mouse in which HA scaffold materials containing hRIFs were subcutaneously transplanted into 4 sites on the dorsal surface. **D** HE and Masson staining of the regenerated collagen tissue in grafts. There were 6 groups: the blank group (HA without cells; $n=6$), the normal control (NC) group (HA with hRIFs; $n=6$), the Len-sh-ctrl group (HA with hRIFs transfected with Len-sh-ctrl; $n=6$), the Len-sh-*KL* group (HA with hRIFs transfected with Len-sh-*KL*; n = 6), the Len- ctrl group (HA with hRIFs transfected with Len-ctrl; $n=6$) and the Len-*KL* group (HA with hRIFs transfected with Len-*KL*; $n=6$)

colocalized with Wnt2 in hRIFs under osteogenic conditions, especially in the cytoplasm (Fig. 5L–M). We further treated hRIFs with pHA-*Wnt2* to overexpress *Wnt2*, which significantly decreased the p-β-catenin/β-catenin ratio and promoted the expression of osteogenic markers in hRIFs under osteogenic conditions (Fig. 5N–P); additionally, coculture with r-KL was able to suppress the osteogenic phenotype of pHA-*Wnt2*-transfected hRIFs that was promoted by activation of the Wnt–β-catenin pathway (Fig. 5N–5P).

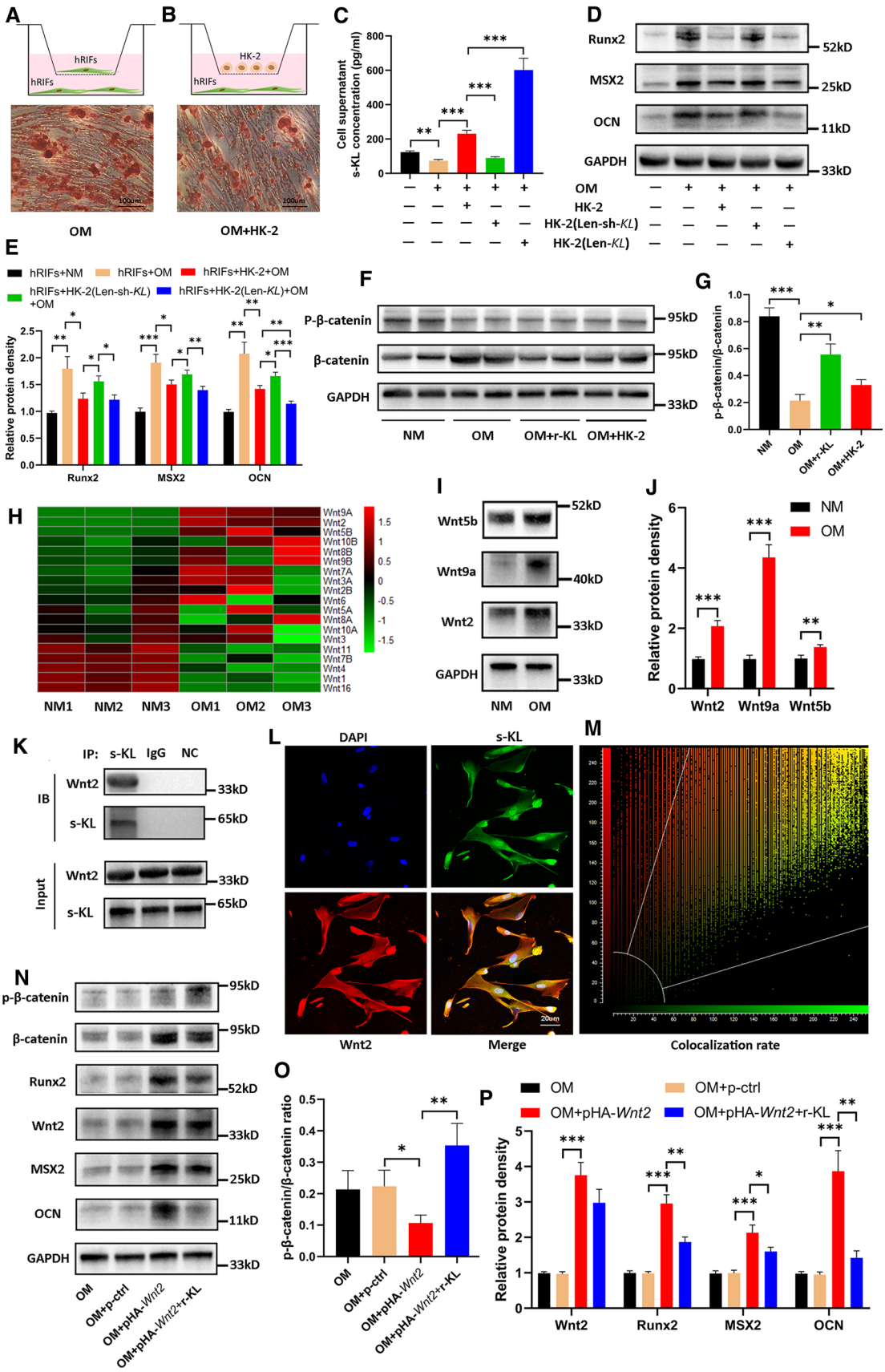
A
hRIFs
hRIFs
OM
B
HK-2
hRIFs
OM+HK-2
C
Cell supernatant s-KL concentration (pg/ml)
OM
HK-2
HK-2(Len-sh-KL)
HK-2(Len-KL)
D
Runx2
MSX2
OCN
GAPDH
52kD
25kD
11kD
33kD
E
hRIFs+NM
hRIFs+OM
hRIFs+HK-2+OM
hRIFs+HK-2(Len-sh-KL)+OM
hRIFs+HK-2(Len-KL)+OM
Relative protein density
Runx2
MSX2
OCN
F
P-β-catenin
β-catenin
GAPDH
95kD
95kD
33kD
NM
OM
OM+r-KL
OM+HK-2
G
p-β-catenin/β-catenin
H
Wnt9A
Wnt2
Wnt5B
Wnt10B
Wnt8B
Wnt9B
Wnt7A
Wnt3A
Wnt2B
Wnt6
Wnt5A
Wnt8A
Wnt10A
Wnt3
Wnt11
Wnt7B
Wnt4
Wnt1
Wnt16
NM1
NM2
NM3
OM1
OM2
OM3
I
Wnt5b
Wnt9a
Wnt2
GAPDH
52kD
40kD
33kD
33kD
NM
OM
J
NM
OM
Relative protein density
Wnt2
Wnt9a
Wnt5b
K
IP: s-KL IgG NC
IB
Wnt2
s-KL
Input
Wnt2
s-KL
33kD
65kD
33kD
65kD
L
DAPI
s-KL
Wnt2
Merge
M
Colocalization rate
N
p-β-catenin
β-catenin
Runx2
Wnt2
MSX2
OCN
GAPDH
95kD
95kD
52kD
33kD
25kD
11kD
33kD
OM
OM+p-ctrl
OM+pHA-Wnt2
OM+pHA-Wnt2+r-KL
O
p-β-catenin/β-catenin ratio
OM
OM+p-ctrl
OM+pHA-Wnt2
OM+pHA-Wnt2+r-KL
P
OM
OM+p-ctrl
OM+pHA-Wnt2
OM+pHA-Wnt2+r-KL
Relative protein density
Wnt2
Runx2
MSX2
OCN

◂**Fig. 5** Soluble α-Klotho (s-KL) released from HK-2 cells inactivated the Wnt–β-catenin pathway to inhibit osteogenic differentiation of human renal interstitial fibroblasts (hRIFs) by binding to Wnt2. **A** Alizarin Red staining (ARS) of monocultured hRIFs ($n=3$) or **B** cocultured hRIFs ($n=3$) with HK-2 cells 14 days after osteogenic induction. HRIFs were cocultured with HK-2 cells transfected with Len-sh-*KL* or Len-*KL,* and **C** The s-KL concentration was determined by ELISA in the cell supernatants; $n=6$. **D–E** Osteogenic markers (OCN, MSX2, Runx2) were evaluated by WB in hRIFs 7 days after osteogenic induction; $n=3$. **F–G** HRIFs were cocultured with recombinant human KL (r-KL) or HK-2 cells in osteogenic medium (OM; 7 days), and the ratio of p-β-catenin to β-catenin was determined by WB; $n=6$. **(H)** A heatmap of Wnt mRNA expression measured by qRT-PCR in hRIFs 7 days after culture with osteogenic medium ($n=3$) or normal medium (NM; $n=3$). **I–J** Representative western blots and quantification of Wnt2, Wnt5b and Wnt9a expression in hRIFs 7 days after culture with OM or NM; $n=3$. **K** Representative western blots of Wnt2 and s-KL in whole-cell lysates of hRIFs and coimmunoprecipitation with anti-s-KL antibodies ($n=3$), IgG ($n=3$) or unconjugated beads ($n=3$) as a negative control (NC). Immunoblotting = IB; immunoprecipitation = IP. **(L)** Fluorescence-labeled Wnt2 (red), s-KL (green) and nuclei (blue) were visualized in hRIFs by confocal microscopy, and **M** the colocalization ratio (78.31%) was calculated by the system; $n=3$. **N–P** Representative western blots and quantification of Wnt2, p-β-catenin, β-catenin and osteogenic marker protein levels in hRIFs that were transfected with or without the Wnt2 plasmid (pHA-Wnt2) and cocultured with or without r-KL; $n=3$

s-KL inactivated the wnt–β-catenin pathway by upregulating secreted frizzled-related protein 1 (SFRP1)

In addition to interacting with Wnt ligands, s-KL has been found to inactivate the Wnt–β-catenin pathway by modulating Wnt inhibitors such as SOST, DKK1 and secreted frizzled-related proteins (SFRPs) [41]. The current results showed that osteogenic induction decreased the mRNA expression of *SFRP1* and increased that of *DKK1* as well as *SFRP4* but did not affect that of *SOST* (Fig. 6A). Further analysis revealed that coculture with r-KL increased the mRNA expression of *SFRP1* and *SFRP4*, but no alteration was noted in DKK1 (Fig. 6A). We also determined the corresponding protein levels using WB and found that the results were consistent with the above results for the mRNA levels (Fig. 6B–C). Subsequently, to determine the effect of SFRP1 and SFRP4 on osteogenic differentiation of hRIFs, the *SFRP1* and *SFRP4* genes were silenced separately with retransfected siRNAs, yielding a decrease of approximately 50–60% in the protein levels 7 days after osteogenic induction (Fig. 6D, G; Supplementary Fig. 3 J–K). Downregulation of SFRP1 significantly decreased the p-β-catenin/β-catenin ratio (Fig. 6D–E) and promoted the expression of osteogenic markers in hRIFs (Fig. 6D, F) despite the lack of change in the SFRP4 protein level (Fig. 6D, Supplementary Fig. 3 J), while downregulation of SFRP4 increased β-catenin expression but failed to influence the p-β-catenin/β-catenin ratio (Fig. 6G–H) and the expression of osteogenic markers (Fig. 6G, I) and showed no effect on the protein level of SFRP1 (Fig. 6G, Supplementary Fig. 3 K). In addition, we further performed coculture with r-KL and hRIFs transfected with si-*SFRP1*. The results showed that si-*SFRP1* partially abolished the inactivation of the Wnt–β-catenin pathway and the suppressed expression of osteogenic markers induced by r-KL (Fig. 6J–L). Collectively, these data suggested that upregulation of SFRP1 was another mechanism through which s-KL inactivated the Wnt–β-catenin pathway to suppress osteogenic differentiation of hRIFs.

HK-2 cells inhibited osteogenic differentiation of hRIFs at least partially via s-KL to inactivate the Wnt–β-catenin pathway

To further verify whether inactivation of the Wnt–β-catenin pathway is one of the key mechanisms through which s-KL released from HK-2 cells attenuates osteogenic differentiation of hRIFs, SKL2001 (20 μM; Selleck, USA), a β-catenin agonist, was cocultured with hRIFs and r-KL in osteogenic medium. The results showed that SKL2001 significantly upregulated β-catenin expression, decreased the p-β-catenin/β-catenin ratio (Fig. 7D–E), and promoted osteogenic differentiation of hRIFs (Fig. 7A–D, F), indicating that SKL2001 weakened the inhibitory effect of s-KL by markedly activating the Wnt–β-catenin pathway. Moreover, a TOPFlash luciferase reporter assay was performed to assess the functional consequence of s-KL on β-catenin-mediated gene transcription. Coculture with r-KL significantly decreased TOPFlash activity in hRIFs in an approximately dose-dependent manner (Fig. 7G). Similarly, coculture with HK-2 cells inhibited TOPFlash activity, and this effect was even stronger by coculture with HK-2 cells transfected with Len-*KL* but was reduced by coculture with HK-2 cells transfected with Len-sh-*KL* (Fig. 7H). The above results indicated that HK-2 cells inhibited osteogenic differentiation of hRIFs at least partially via s-KL to inactivate the Wnt–β-catenin pathway (Fig. 8A).

The Wnt–β-catenin pathway was activated in RP tissues

To further evaluate whether the Wnt–β-catenin pathway is activated in RP tissues, we evaluated the p-β-catenin/β-catenin ratio as well as inhibitors of the Wnt–β-catenin pathway, including SFRP1, SFRP4, DKK1 and SOST. Surprisingly, the p-β-catenin/β-catenin ratio was significantly decreased in RP tissues compared to NRP tissues (Fig. 7I–M), suggesting that the Wnt–β-catenin pathway was activated. In addition, the expression of SFRP1 and DKK1 was markedly suppressed (Fig. 7I–K, M), but no significant difference was noted in the expression of SFRP4 and

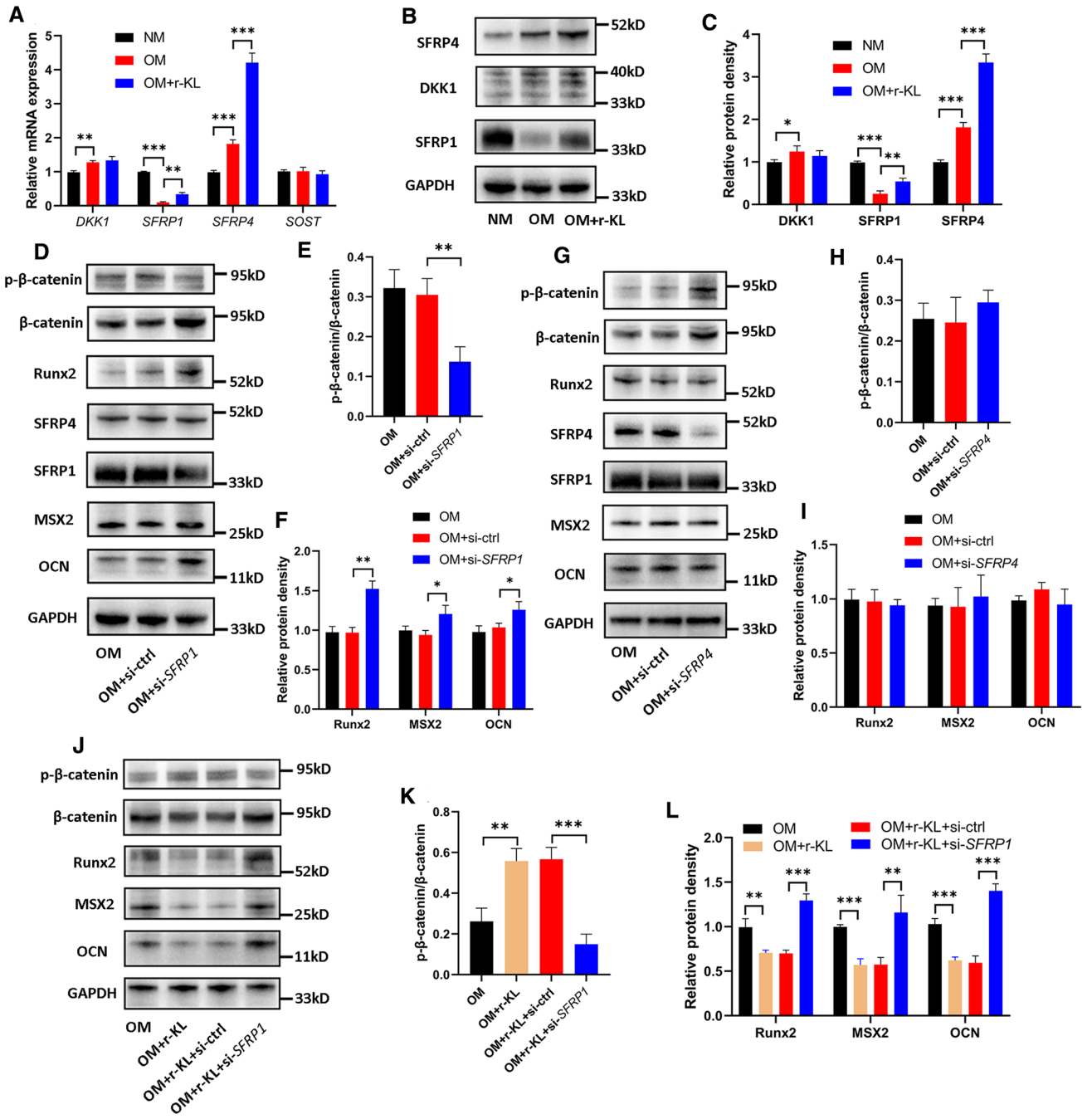

Fig. 6 Soluble α-Klotho (s-KL) inactivated the Wnt–β-catenin pathway by upregulating secreted frizzled-related protein 1 (SFRP1). Human renal interstitial fibroblasts (hRIFs) were cultured alone in normal medium (NM) or osteogenic medium (OM) or were cocultured with recombinant KL (r-KL) in OM for 7 days ($n=3$), and **A** qRT-PCR was performed to determine the relative mRNA expression levels of *DKK1*, *SFRP1*, *SFRP4*, and *SOST*, and **B–C** WB was performed to determine their relative protein expression levels. **D–F** HRIFs were retransfected with siRNAs targeting *SFRP1* and induced with OM for 7 days ($n=3$), and WB was used to determine the relative protein levels of SFRP1, SFRP4, p-β-catenin, β-catenin and osteogenic markers (OCN, MSX2, Runx2). **G–I** HRIFs were retransfected with siRNAs targeting *SFRP4* and induced with OM for 7 days ($n=3$), and WB was used to determine the relative protein levels of SFRP4, SFRP1, p-β-catenin, β-catenin and osteogenic markers. **(J–L)** HRIFs were cotransfected with siRNAs targeting *SFRP1* and cocultured with r-KL under osteogenic conditions for 7 days ($n=3$), and WB was used to determine the relative protein levels of p-β-catenin, β-catenin and osteogenic markers

SOST (Fig. 7I–K,M). Furthermore, linear regression analysis revealed that the s-KL expression level was positively correlated with the p-β-catenin/β-catenin ratio (Fig. 7N), that SFRP1 was negatively correlated with Runx2 (Fig. 7O, Supplementary Fig. 4A–B), and that DKK1 was negatively correlated with OCN (Fig. 7P, Supplementary Fig. 4C–D). Despite the lack of statistical significance, notably, there was a trend toward a positive correlation of s-KL expression with that of Wnt–β-catenin pathway inhibitors such as SFRP1 (Fig. 7Q) and DKK1 (Fig. 7R); in addition, the p-β-catenin/β-catenin ratio was positively correlated with the expression levels of SFRP1 (Supplementary Fig. 4E–F) and inversely correlated with osteogenic markers (Supplementary Fig. 4G–I). Regarding the linear regression analysis of the m-KL expression level and p-β-catenin/β-catenin ratio as well as the expression levels of pathway inhibitors, no significant correlations were identified (Supplementary Fig. 4 J–L), although there was a positive correlation between the m-KL and s-KL levels (Supplementary Fig. 2B). Collectively, our study provides insight suggesting that deficiency of s-KL might release the repression of Wnt–β-catenin pathway to mediate osteogenic-like processes prior to RP formation (Fig. 8).

Discussion

Though the surgical management of renal stones has been largely improved by instrument miniaturization, no substantial changes have been made over the past several decades due to the very limited understanding of the pathophysiological mechanisms underlying stone formation [42]. CaOx stones were identified to originate from RP, resembling ectopic calcification, and increasing numbers of studies have highlighted the important roles of the process driven by osteogenic-like cells [8]. Both human renal tubular epithelial cells and hRIFs have been found to adopt an osteogenic phenotype, and CaP depositions have been detected in cell layers after treatment with standard osteogenic media [10, 29]. Moreover, spontaneous calcification was observed in pericyte-like primary renal cells isolated from a patient with medullary sponge kidney after 4–5 months in culture. However, the pathophysiological mechanisms initiating or promoting the osteogenic process remain elusive.

Given the proven inhibitory roles of KL in ectopic calcification [15] and the identified association between urolithiasis and the G-395A gene polymorphism [26], we first investigated the expression of KL in RP and NRP tissues and found that both s-KL and m-KL were significantly downregulated and that the protein level of s-KL was inversely correlated with that of MSX2 in RP, consistent with the significant downregulation of s-KL observed in hRIFs and HK-2 cells induced with osteogenic medium and indicating the potential role of s-KL in RP formation. In addition, we observed that the abundance of s-KL was markedly lower in hRIFs cultured in normal medium, that hRIFs had a more significant decrease in the s-KL level than did HK-2 cells after osteogenic induction, and that the osteogenic capacity of hRIFs was greater than that of HK-2 cells. Thus, we hypothesized the potential role of s-KL in hRIF osteogenic differentiation and further verified its inhibitory role in vitro and in vivo. Furthermore, considering the high expression of s-KL in renal tubular epithelial cells, we cocultured hRIFs with r-KL and HK-2 cells. Our results showed that both r-KL and HK-2 cells played an inhibitory role in osteogenic differentiation of hRIFs. Additionally, coculture with HK-2 cells significantly increased the cell supernatant concentration of s-KL, while coculture with HK-2 cells transfected with Lensh-*KL* decreased the cell supernatant concentration of s-KL and abolished its inhibitory effect, emphasizing that HK-2 cells inhibit osteogenic differentiation of hRIFs at least partially by releasing s-KL.

KL has been reported to play an inhibitory role in ectopic calcification by regulating various signaling pathways [25, 43, 44]. Thereinto, the Wnt–β-catenin pathway has been established as a key regulator of osteogenesis [39], and our previous study confirmed that activation of the Wnt–β-catenin pathway triggered osteogenic differentiation of hRIFs [45]. This study further revealed that s-KL was able to inactivate the Wnt–β-catenin pathway partially by binding to Wnt2 in the intracellular space. Similarly, previous studies found that s-KL/m-KL function as Wnt antagonists by binding to Wnt1 [27, 34, 46], Wnt3 [34], Wnt3a [46], Wnt4 [27, 34], Wnt5a [34], Wnt7a [27] and Wnt10b [47], suggesting that KL plays a vital role in the regulation of the Wnt–β-catenin pathway by binding to multiple Wnt ligands. Moreover, the direct interaction of s-KL and Wnt1 has been reported to be detectable in culture medium using Co-IP [27], indicating that binding of s-KL and Wnt ligands also occurs in the extracellular space. Our study demonstrated the direct interaction of s-KL and Wnt2 in hRIFs and the inhibitory role of extracellular r-KL in Wnt–β-catenin pathway activated by overexpressing Wnt2, in combination with a previous study reporting that extracellular s-KL could attenuate Wnt–β-catenin signaling activated by extracellular Wnt3a but failed to play an inhibitory role in Wnt–β-catenin signaling directly activated by upregulation of intracellular β-catenin [34], which led us to speculate that s-KL might directly bind to Wnt2 in the extracellular space, the mechanism through which both s-KL from HK-2 cells and r-KL inactivated the Wnt–β-catenin pathway in hRIFs (Fig. 8A). However, well-designed studies are anticipated to explore whether this extracellular interaction exists.

Alternatively, in terms of the effect of s-KL on Wnt inhibitors, a previous study reported that fibroblast growth factor 23 (FGF23) and s-KL synergistically contributed to

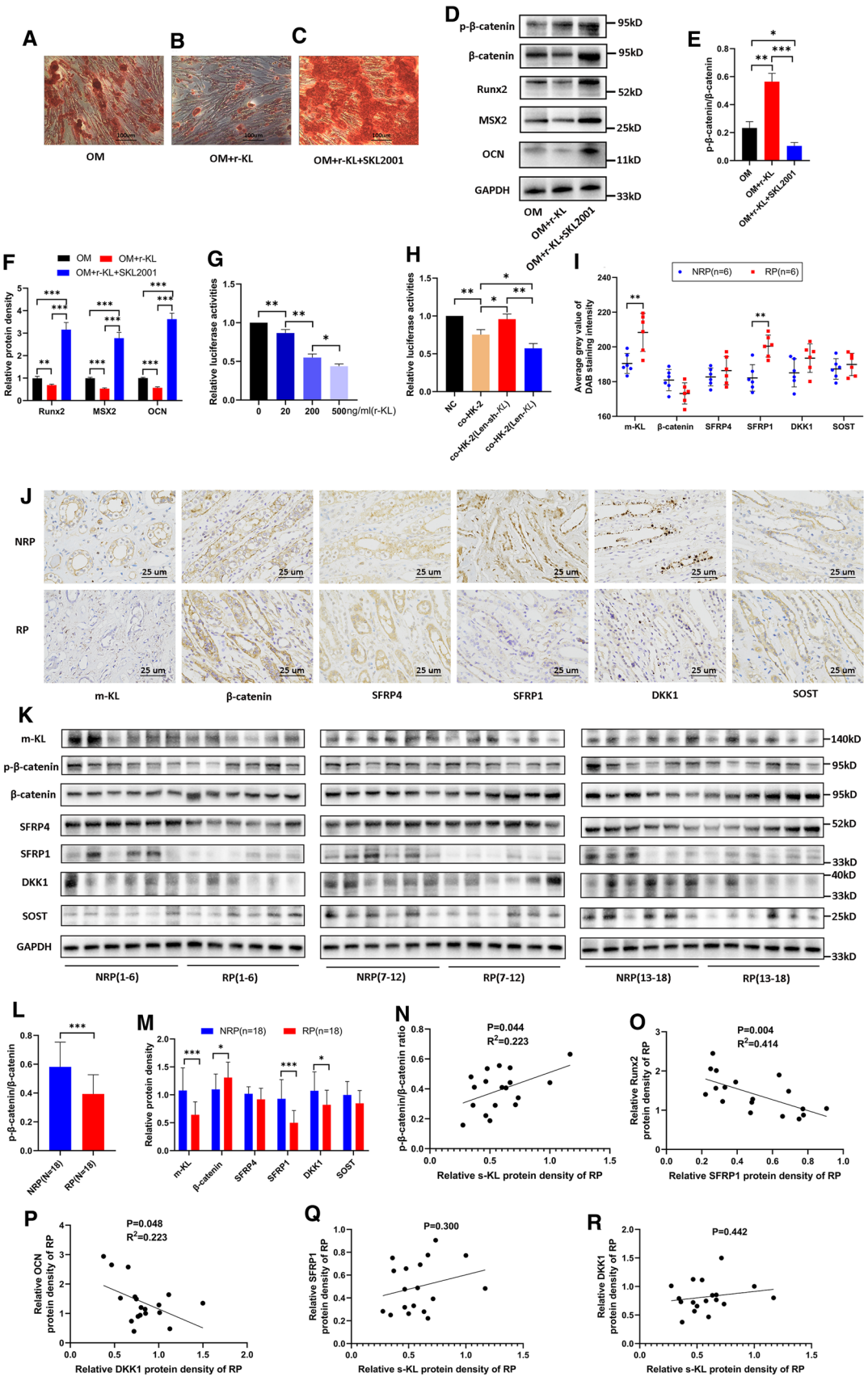
A
B
C
OM
OM+r-KL
OM+r-KL+SKL2001
D
p-β-catenin
β-catenin
Runx2
MSX2
OCN
GAPDH
95kD
95kD
52kD
25kD
11kD
33kD
OM
OM+r-KL
OM+r-KL+SKL2001
E
p-β-catenin/β-catenin
F
OM
OM+r-KL
OM+r-KL+SKL2001
Relative protein density
Runx2
MSX2
OCN
G
Relative luciferase activities
0
20
200
500ng/ml(r-KL)
H
Relative luciferase activities
NC
co-HK-2
co-HK-2(Len-sh-KL)
co-HK-2(Len-KL)
I
NRP(n=6)
RP(n=6)
Average grey value of DAB staining intensity
m-KL
β-catenin
SFRP4
SFRP1
DKK1
SOST
J
NRP
RP
25 um
m-KL
β-catenin
SFRP4
SFRP1
DKK1
SOST
K
m-KL
p-β-catenin
β-catenin
SFRP4
SFRP1
DKK1
SOST
GAPDH
140kD
95kD
95kD
52kD
33kD
40kD
33kD
25kD
33kD
NRP(1-6)
RP(1-6)
NRP(7-12)
RP(7-12)
NRP(13-18)
RP(13-18)
L
p-β-catenin/β-catenin
NRP(N=18)
RP(N=18)
M
NRP(n=18)
RP(n=18)
Relative protein density
m-KL
β-catenin
SFRP4
SFRP1
DKK1
SOST
N
P=0.044
R²=0.223
p-β-catenin/β-catenin ratio
Relative s-KL protein density of RP
O
P=0.004
R²=0.414
Relative Runx2 protein density of RP
Relative SFRP1 protein density of RP
P
P=0.048
R²=0.223
Relative OCN protein density of RP
Relative DKK1 protein density of RP
Q
P=0.300
Relative SFRP1 protein density of RP
Relative s-KL protein density of RP
R
P=0.442
Relative DKK1 protein density of RP
Relative s-KL protein density of RP

◂**Fig. 7** HK-2 cells inhibited osteogenic differentiation of human renal interstitial fibroblasts (hRIFs) at least partially via soluble α-Klotho (s-KL) to inactivate the Wnt–β-catenin pathway, and the Wnt–β-catenin pathway was activated in Randall's plaques (RP). HRIFs were cocultured with recombinant KL (r-KL) or the β-catenin agonist SKL2001 (20 μM). **A–C** Alizarin Red staining (ARS) of calcium deposits 14 days after osteogenic induction ($n=3$). **D–F** WB was used to determine the relative protein levels of p-β-catenin, β-catenin and osteogenic markers (OCN, MSX2, Runx2) 7 days after osteogenic induction ($n=3$). HRIFs were cotransfected with the TOPFlash plasmid and the Renilla luciferase plasmid as an internal control. **G** The relative luciferase activity was determined in transfected hRIFs cocultured with different concentrations of r-KL under osteogenic conditions for 48 h ($n=3$). **H** The relative luciferase activity was determined in transfected hRIFs cocultured with HK-2 cells, Len-sh-KL-transfected HK-2 cells or Len-KL-transfected HK-2 cells under osteogenic conditions for 48 h ($n=3$). **I–J** Immunohistochemistry (IHC) for transmembrane KL (m-KL), β-catenin and Wnt–β-catenin pathway inhibitors (SFRP4, SFRP1, DKK1, and SOST) in RP ($n=6$) and normal renal papillae (NRP; $n=6$); the DAB staining density was quantified by the average gray value using the IHC Toolbox plugin in ImageJ. **K–M** Representative western blots and quantification of m-KL, the ratio of p-β-catenin to β-catenin and Wnt–β-catenin pathway inhibitors in RP ($n=18$) and NRP ($n=18$) tissues. **N–R** Correlation analysis between the relative protein expression level of s-KL and the ratio of p-β-catenin to β-catenin **N**, the expression levels of SFRP1 and Runx2 **O**, the expression levels of DKK1 and OCN **P**, the expression levels of s-KL and SFRP1 **Q**, and the expression levels of s-KL and DKK1 **R** in RP tissues; $n=18$

bone loss secondary to chronic disease through induction of Dkk1 and inactivation of the Wnt–β-catenin pathway [41]. In contrast, this study revealed that upregulation of SFRP1 instead of DKK1 was another mechanism through which s-KL inactivated the Wnt–β-catenin pathway and thus attenuated osteogenic differentiation of hRIFs. Intriguingly, our study further identified the activated Wnt–β-catenin pathway and decreased expression of its inhibitors (SFRP1 and DKK1) in RP tissues, and the s-KL expression level was inversely associated with the p-β-catenin/β-catenin ratio. Notably, despite the lack of statistical significance, probably due to the limited number of samples, there was a trend toward a positive correlation of the s-KL level with those of SFRP1 and DKK1, and the p-β-catenin/β-catenin ratio was positively correlated with the expression levels of SFRP1 and inversely correlated with osteogenic markers. These results indicated that deficiency of s-KL might release the repression of Wnt–β-catenin pathway to mediate renal interstitium biomineralization and, thus, contribute to RP formation. Moreover, loss of KL was found to contribute to kidney injury, in which the Wnt–β-catenin pathway was also pathologically enhanced [27], and the role of immunity and inflammation in RP formation has been highlighted [48]. Collectively, our results and those of these studies indicate that it is promising to further clarify a potential core role of s-KL in the complex mechanism of RP formation via regulation of the Wnt–β-catenin pathway. Additionally, as s-KL generated from the proteolytic cleavage of m-KL [20], it was not surprising that m-KL was also found to be downregulated in RP. Notably, m-KL was identified to inhibit the renal phosphate reabsorption in cooperation with FGF23 [49, 50], and thus m-KL deficiency might impair the phosphate and calcium homeostasis in renal papillae to facilitate renal interstitium biomineralization, despite no correlation between m-KL and osteogenic markers was found in this study. The deficiency of m-KL and s-KL might synergically contribute to RP formation, and this putative effect is yet to be experimentally confirmed.

Of note, there was a trend toward downregulation of UKCR in CaOx-SF compared with HC, but the difference was not significant. This trend may be caused by the considerable heterogeneity of urinary s-KL levels among CaOx-SF and the limited number of cases analyzed in this study. On the other hand, it has been shown that circulating s-KL is not filtered across the glomerular barrier; thus, urinary s-KL is tubular in origin [37]. The lack of correlation between s-KL changes in urine and RP tissues may be explained by the observation that the decreased level of s-KL might only occur in the limited amount of RP tissues instead of the extensive population of renal tubular epithelial cells, since there are a large number of idiopathic CaOx stone-forming patients with normal renal function, and urinary s-KL has been reported to be closely associated with renal function [50]. Importantly, a previous study compared the serum s-KL level among renal stone patients with hypercalciuria, stone patients without hypercalciuria and healthy subjects [51], and no significant difference was observed among the three groups. Therefore, further studies with larger samples are needed to clarify the change in urinary s-KL levels in RP formers.

This study focused on the effect of s-KL released from renal tubular epithelial cells on osteogenic differentiation of hRIFs, and it is also important to further determine what and how influence the expression of KL in tubular epithelial cells or the s-KL released from these cells. It has been established that an abnormal environment created by hyperoxaluria, hypercalciuria, hyperphosphaturia and hypocitraturia plays a critical role in stone formation [48], although the mechanism remains unclear. Given the direct exposure of tubular epithelial cells to lithogenic conditions in renal tubules, these lithogenic conditions might contribute to the downregulation of KL in tubular epithelial cells. Additionally, urinary exosomes carrying s-KL have been found to participate in renal disorders such as renal injury [52]. Interestingly, a recent study determined the proteins carried in urinary exosomes from primary hyperoxaluria type 1 (PH1) patients with nephrocalcinosis ($n=6$), with CaOx stones ($n=9$) or with neither disease process ($n=10$), which showed that the s-KL density in patients with PH1 and nephrocalcinosis and patients with PH1 and CaOx stones were significantly lower than that of patients with PH1 with neither disease

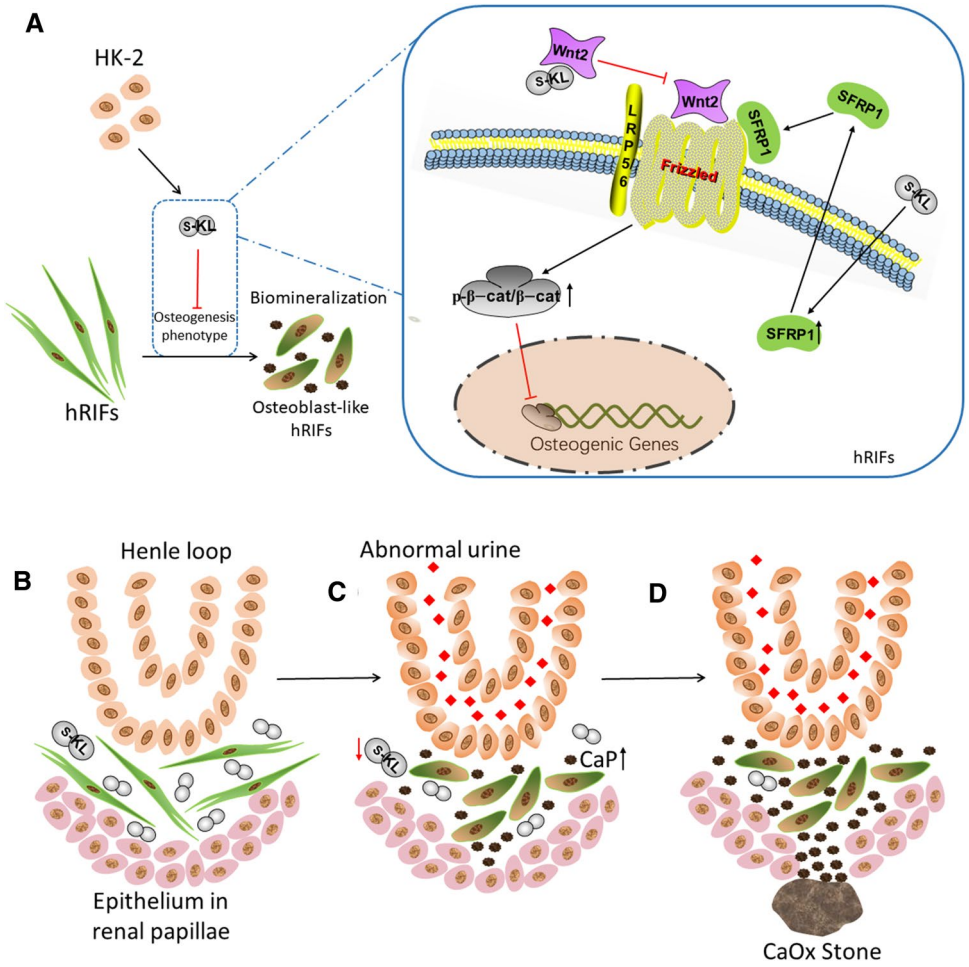

Fig. 8 A schematic model of the potential mechanism by which soluble α-Klotho (s-KL) released from HK-2 cells inhibits osteogenic differentiation of renal interstitial fibroblasts (hRIFs) and the hypothetical partial process of Randall's plaque (RP) formation based on our findings. **A** s-KL released from HK-2 cells inactivates the Wnt–β-catenin pathway to inhibit osteogenic differentiation of hRIFs by directly binding to Wnt2 and upregulating SFRP1. **B** A normal renal papilla. **C** An abnormal urinary environment, such as hyperoxaluria, hypercalciuria, hyperphosphaturia and hypocitraturia, might decrease the level of interstitial s-KL released from renal tubular epithelial cells, which compromises the protective role of tubular epithelial cells in hRIFs exposed to osteogenic conditions. Multiple pathological factors synergically promote hRIFs to adopt an osteogenic phenotype and lead to the formation of calcium phosphate (CaP) deposits in the renal interstitium. **D** Aggregations of CaP breach the covering epithelium in renal papillae to form RP, which act as a nidus for calcium oxalate (CaOx) stone formation

process [53]. Therefore, identifying the crosstalk or interaction between renal tubular epithelial cells and interstitial cells via exosomes carrying s-KL is expected to facilitate the understanding of the mechanism underlying RP formation (Fig. 8).

Regrettably, it remains challenging to identify the receptor for circulating s-KL, which has led to the lack of efficient and specific inhibitors to block s-KL activity [21]. In addition, most animal models have a unipapillary system that is different from the multipapillary system in humans; studies in animal models have shown that hyperoxaluria and hypercalciuria lead to intratubular but not interstitial deposits and that intratubular deposits can move into the interstitium but are eventually eliminated [54, 55]. Thus, experimental research on RP formation has been slowed largely due to the lack of ideal established animal models. Although this study innovatively evaluated the role of s-KL in hRIF osteogenic differentiation in vivo via subcutaneous ectopic transplantation, we have to acknowledge the main limitations that the subcutaneous microenvironment is significantly different from that of the papillary renal interstitium, and we tried but failed to perform IHC of transplanted grafts for other osteogenic markers, such as OCN, MSX2, Runx2, and ALP. Despite these limitations, this study provided novel insights into the pathogenesis of idiopathic CaOx stones, and further investigations based on an ideal RP animal model are anticipated.

Conclusions

This study showed that deficiency of s-KL was a pathological feature of the osteogenic-like process of RP formation, and revealed that s-KL released from HK-2 cells suppressed the activation of the Wnt–β-catenin pathway to play an inhibitory role in osteogenic differentiation of hRIFs, at least partially through binding to Wnt2 and upregulating SFRP1. Further investigations in RP tissues indicated that the deficiency of s-KL might release the repression of Wnt–β-catenin pathway and thus contribute to RP formation. Our study not only provided in-depth insight into the role of s-KL in renal interstitial biomineralization but also shed new light on the interaction of renal tubular epithelial cells and interstitial cells to clarify the complex mechanisms of RP formation. However, further studies based on an ideal animal model are needed to comprehensively clarify the potential role of KL in RP formation, which may be helpful to find a novel and effective approach for the prevention of CaOx stones.

Supplementary Information The online version contains supplementary material available at https://doi.org/10.1007/s00018-021-03972-x.

Acknowledgements Thank National Natural Science Foundation of China, Natural Science Foundation of Hunan Province for providing funding for this study and Central South University Independent Exploration and Innovation Project for Graduate Students.

Author contributions ZZ, ZC and HC performed study concept and designed the experiment. ZZ, SR, YJ, FH, WX, JC, YC, CH and FZ contributed to the development of methodology and the acquisition of data. ZZ, YL and ZC contributed to analysis and interpretation of data. ZZ, ZC and HC contributed to writing and revision of the manuscript. ZZ, YC and HC contributed to the administrative, technical and material support. ZC and HC contributed to study supervision. All authors read and approved the final paper.

Funding This work was supported by the National Natural Science Foundation of China (81770705 to Hequn Chen; 82000761 to Yu Cui); Natural Science Foundation of Hunan Province (2019JJ40488 to Zhiyong Chen); Central South University Independent Exploration and Innovation Project for Graduate Students (2021zzts0348 to Zewu Zhu).

Data availability The datasets used and/or analyzed during this study are available from the corresponding author on reasonable request.

Declarations

Conflict of interests The authors declare that they have no competing interests.

Ethics approval Approval was granted by Xiangya Hospital Ethics Committee (Approval Number: 202103089) and the Institutional Experimental Animal Committee of Central South University (Proof Number: 2021sydw0033).

Consent to participate Written informed consents for surgical procedures and getting samples were obtained from all included patients prior to surgery. The study was performed in accordance with the Declaration of Helsinki.

Consent for publication Written informed consents for publishing clinical characteristics on the condition of anonymity were obtained from all included patients.

References

1. Turney BW, Reynard JM, Noble JG and Keoghane SR (2012) Trends in urological stone disease. BJU Int 109: 1082-+. DOI: https://doi.org/10.1111/j.1464-410X.2011.10495.x.
2. Neisius A, Preminger GM (2013) Epidemiology, prevention and redefining therapeutic standards. Nat Rev Urol 10:75–77. https://doi.org/10.1038/nrurol.2012.253
3. Heers H, Turney BW (2016) Trends in urological stone disease: a 5-year update of hospital episode statistics. BJU Int 118:785–789. https://doi.org/10.1111/bju.13520
4. Canales BK, Hatch M (2014) Kidney stone incidence and metabolic urinary changes after modern bariatric surgery: review of clinical studies, experimental models, and prevention strategies. Surg Obes Related Dis 10:734–742. https://doi.org/10.1016/j.soard.2014.03.026
5. Evan AP (2010) Physiopathology and etiology of stone formation in the kidney and the urinary tract. Pediatric Nephrol (Berlin, Germany) 25:831–841. https://doi.org/10.1007/s00467-009-1116-y
6. Darves-Bornoz A, Marien T, Thomas J et al (2019) Renal papillary mapping and quantification of randall's plaque in pediatric calcium oxalate stone formers. J Endourol 33:863–867. https://doi.org/10.1089/end.2019.0377
7. Randall A (1937) The origin and growth of renal calculi. Annals Surg 105:1009–1027. https://doi.org/10.1097/00000658-193706000-00014
8. Khan SR, Canales BK (2015) Unified theory on the pathogenesis of Randall's plaques and plugs. Urolithiasis 43(Suppl 1):109–123. https://doi.org/10.1007/s00240-014-0705-9
9. Evan AP, Worcester EM, Coe FL, Williams J Jr, Lingeman JE (2015) Mechanisms of human kidney stone formation. Urolithiasis 43(Suppl 1):19–32. https://doi.org/10.1007/s00240-014-0701-0
10. Priante G, Ceol M, Gianesello L et al (2019) Human proximal tubular cells can form calcium phosphate deposits in osteogenic culture: role of cell death and osteoblast-like transdifferentiation. Cell death discovery 5:57. https://doi.org/10.1038/s41420-019-0138-x
11. Gay C, Letavernier E, Verpont MC et al (2020) Nanoscale analysis of randall's plaques by electron energy loss spectromicroscopy: insight in early biomineral formation in human kidney. ACS Nano 14:1823–1836. https://doi.org/10.1021/acsnano.9b07664
12. Khan SR and Gambaro G (2016) Role of osteogenesis in the formation of randall's plaques. Anatomical record (Hoboken, NJ : 2007) 299: 5–7. DOI: https://doi.org/10.1002/ar.23275.
13. Kuro-o M, Matsumura Y, Aizawa H et al (1997) Mutation of the mouse klotho gene leads to a syndrome resembling ageing. Nature 390:45–51. https://doi.org/10.1038/36285
14. Xu Y, Sun Z (2015) Molecular basis of Klotho: from gene to function in aging. Endocrine Rev 36:174–193. https://doi.org/10.1210/er.2013-1079
15. Lindberg K, Amin R, Moe OW et al (2014) The kidney is the principal organ mediating klotho effects. J Am Soc Nephrol 25:2169–2175. https://doi.org/10.1681/asn.2013111209
16. Li SA, Watanabe M, Yamada H et al (2004) Immunohistochemical localization of Klotho protein in brain, kidney, and reproductive

organs of mice. Cell Struct Funct 29:91–99. https://doi.org/10.1247/csf.29.91
17. Chen CD, Podvin S, Gillespie E, Leeman SE, Abraham CR (2007) Insulin stimulates the cleavage and release of the extracellular domain of Klotho by ADAM10 and ADAM17. Proc Natl Acad Sci U S A 104:19796–19801. https://doi.org/10.1073/pnas.0709805104
18. Imura A, Iwano A, Tohyama O et al (2004) Secreted Klotho protein in sera and CSF: implication for post-translational cleavage in release of Klotho protein from cell membrane. FEBS Lett 565:143–147. https://doi.org/10.1016/j.febslet.2004.03.090
19. Mencke R, Harms G, Moser J, et al (2017) Human alternative Klotho mRNA is a nonsense-mediated mRNA decay target inefficiently spliced in renal disease. JCI insight 2. DOI: https://doi.org/10.1172/jci.insight.94375
20. Saar-Kovrov V, Donners M, van der Vorst EPC (2020) Shedding of klotho: functional implications in chronic kidney disease and associated vascular disease. Front Cardiovasc Med 7:617842. https://doi.org/10.3389/fcvm.2020.617842
21. Dalton GD, Xie J, An SW, Huang CL (2017) New insights into the mechanism of action of soluble klotho. Front Endocrinol 8:323. https://doi.org/10.3389/fendo.2017.00323
22. Kurosu H, Yamamoto M, Clark JD et al (2005) Suppression of aging in mice by the hormone Klotho. Science (New York, NY) 309:1829–1833. https://doi.org/10.1126/science.1112766
23. Masuda H, Chikuda H, Suga T, Kawaguchi H, Kuro-o M (2005) Regulation of multiple ageing-like phenotypes by inducible klotho gene expression in klotho mutant mice. Mech Ageing Dev 126:1274–1283. https://doi.org/10.1016/j.mad.2005.07.007
24. Li F, Yao Q, Ao L et al (2017) Klotho suppresses high phosphate-induced osteogenic responses in human aortic valve interstitial cells through inhibition of Sox9. J Mol Med (Berlin, Germany) 95:739–751. https://doi.org/10.1007/s00109-017-1527-3
25. Zhang W, Xue D, Hu D et al (2015) Secreted klotho protein attenuates osteogenic differentiation of human bone marrow mesenchymal stem cells in vitro via inactivation of the FGFR1/ERK signaling pathway. Growth factors (Chur, Switzerland) 33:356–365. https://doi.org/10.3109/08977194.2015.1108313
26. Zhu Z, Xia W, Cui Y et al (2019) Klotho gene polymorphisms are associated with healthy aging and longevity: evidence from a meta-analysis. Mech Ageing Dev 178:33–40. https://doi.org/10.1016/j.mad.2018.12.003
27. Zhou L, Li Y, Zhou D, Tan RJ, Liu Y (2013) Loss of Klotho contributes to kidney injury by derepression of Wnt/β-catenin signaling. J Am Soc Nephrol 24:771–785. https://doi.org/10.1681/asn.2012080865
28. Evan AP, Coe FL, Lingeman J, Bledsoe S, Worcester EM (2018) Randall's plaque in stone formers originates in ascending thin limbs. Am J Physiol Renal Physiol 315:F1236-f1242. https://doi.org/10.1152/ajprenal.00035.2018
29. Zhu Z, Huang F, Xia W et al (2020) Osteogenic differentiation of renal interstitial fibroblasts promoted by lncRNA MALAT1 may partially contribute to randall's plaque formation. Front Cell Dev Biol 8:596363. https://doi.org/10.3389/fcell.2020.596363
30. Huang Y, Zheng Y, Jia L, Li W (2015) Long noncoding RNA H19 promotes osteoblast differentiation via TGF-beta1/Smad3/HDAC signaling pathway by deriving miR-675. Stem Cells (Dayton, Ohio) 33:3481–3492. https://doi.org/10.1002/stem.2225
31. Yamazaki Y, Imura A, Urakawa I et al (2010) Establishment of sandwich ELISA for soluble alpha-Klotho measurement: Age-dependent change of soluble alpha-Klotho levels in healthy subjects. Biochem Biophys Res Commun 398:513–518. https://doi.org/10.1016/j.bbrc.2010.06.110
32. Shen K, Vesey DA, Ellis RJ et al (2019) GRP78 expression in tumor and perinephric adipose tissue is not an optimal risk stratification marker for clear cell renal cell carcinoma. PLoS ONE 14:e0210246. https://doi.org/10.1371/journal.pone.0210246
33. Shu J, Dolman GE, Duan J, Qiu G, Ilyas M (2016) Statistical colour models: an automated digital image analysis method for quantification of histological biomarkers. Biomed Eng Online 15:46. https://doi.org/10.1186/s12938-016-0161-6
34. Liu H, Fergusson MM, Castilho RM et al (2007) Augmented Wnt signaling in a mammalian model of accelerated aging. Science (New York, NY) 317:803–806. https://doi.org/10.1126/science.1143578
35. Li H, Zhou J, Zhu M et al (2020) Low-intensity pulsed ultrasound promotes the formation of periodontal ligament stem cell sheets and ectopic periodontal tissue regeneration. J Biomed Materials Res Part A. https://doi.org/10.1002/jbm.a.37102
36. Pillai ICL, Li S, Romay M et al (2017) Cardiac fibroblasts adopt osteogenic fates and can be targeted to attenuate pathological heart calcification. Cell Stem Cell 20(218–232):e215. https://doi.org/10.1016/j.stem.2016.10.005
37. Hu MC, Shi M, Zhang J et al (2016) Renal Production, Uptake, and Handling of Circulating αKlotho. J Am Soc Nephrol 27:79–90. https://doi.org/10.1681/asn.2014101030
38. Khan SR (2015) The role of Randall's plaques in urolithiasis. Foreword Urolithiasis 43(Suppl 1):1–3. https://doi.org/10.1007/s00240-014-0721-9
39. Houschyar KS, Tapking C, Borrelli MR et al (2018) Wnt pathway in bone repair and regeneration—What Do We Know So Far. Front Cell Dev Biol 6:170. https://doi.org/10.3389/fcell.2018.00170
40. Chen D, Xie R, Shu B et al (2019) Wnt signaling in bone, kidney, intestine, and adipose tissue and interorgan interaction in aging. Ann New York Acad Sci 1442:48–60. https://doi.org/10.1111/nyas.13945
41. Carrillo-López N, Panizo S, Alonso-Montes C et al (2016) Direct inhibition of osteoblastic Wnt pathway by fibroblast growth factor 23 contributes to bone loss in chronic kidney disease. Kidney Int 90:77–89. https://doi.org/10.1016/j.kint.2016.01.024
42. Thongprayoon C, Krambeck AE, Rule AD (2020) Determining the true burden of kidney stone disease. Nat Rev Nephrol 16:736–746. https://doi.org/10.1038/s41581-020-0320-7
43. Chen J, Lin Y, Sun Z (2016) Deficiency in the anti-aging gene Klotho promotes aortic valve fibrosis through AMPKα-mediated activation of RUNX2. Aging Cell 15:853–860. https://doi.org/10.1111/acel.12494
44. Gu Y, Ren K, Wang L, Yao Q (2019) Loss of Klotho contributes to cartilage damage by derepression of canonical Wnt/β-catenin signaling in osteoarthritis mice. Aging 11:12793–12809. https://doi.org/10.18632/aging.102603
45. Zhu Z, Cui Y, Huang F et al (2020) Long non-coding RNA H19 promotes osteogenic differentiation of renal interstitial fibroblasts through Wnt-β-catenin pathway. Mol Cell Biochem 470:145–155. https://doi.org/10.1007/s11010-020-03753-3
46. Liu Q, Zhu LJ, Waaga-Gasser AM et al (2019) The axis of local cardiac endogenous Klotho-TGF-β1-Wnt signaling mediates cardiac fibrosis in human. J Mol Cell Cardiol 136:113–124. https://doi.org/10.1016/j.yjmcc.2019.09.004
47. Miao J, Liu J, Niu J et al (2019) Wnt/β-catenin/RAS signaling mediates age-related renal fibrosis and is associated with mitochondrial dysfunction. Aging Cell 18:e13004. https://doi.org/10.1111/acel.13004
48. Khan SR, Canales BK, Dominguez-Gutierrez PR (2021) Randall's plaque and calcium oxalate stone formation: role for immunity and inflammation. Nat Rev Nephrol. https://doi.org/10.1038/s41581-020-00392-1
49. Hu MC, Shi M, Moe OW (2019) Role of alphaKlotho and FGF23 in regulation of type II Na-dependent phosphate

co-transporters. Pflugers Arch 471:99–108. https://doi.org/10.1007/s00424-018-2238-5
50. Kuro OM (2019) The Klotho proteins in health and disease. Nat Rev Nephrol 15:27–44. https://doi.org/10.1038/s41581-018-0078-3
51. Melo TL, Esper PLG, Zambrano LI et al (2020) Expression of vitamin D receptor, CYP27B1 and CYP24A1 hydroxylases and 1,25-dihydroxyvitamin D(3) levels in stone formers. Urolithiasis 48:19–26. https://doi.org/10.1007/s00240-019-01163-9
52. Grange C, Papadimitriou E, Dimuccio V et al (2020) Urinary Extracellular Vesicles Carrying Klotho Improve the Recovery of Renal Function in an Acute Tubular Injury Model. Mol Therapy 28:490–502. https://doi.org/10.1016/j.ymthe.2019.11.013
53. Wang N, Ma J, Ren Y, Xiang S, Jia R (2019) Urinary extracellular vesicles carrying klotho improve the recovery of renal function in an acute tubular injury model. Am J Trans Res 11:3375–3383
54. Wu XR (2015) Interstitial calcinosis in renal papillae of genetically engineered mouse models: relation to Randall's plaques. Urolithiasis 43(Suppl 1):65–76. https://doi.org/10.1007/s00240-014-0699-3
55. Khan SR, Canales BK (2011) Ultrastructural investigation of crystal deposits in Npt2a knockout mice: are they similar to human Randall's plaques? J Urol 186:1107–1113. https://doi.org/10.1016/j.juro.2011.04.109